Ann. Geophys. Discuss., https://doi.org/10.5194/angeo-2018-137
Manuscript under review for journal Ann. Geophys.
Discussion started: 23 January 2019
© Author(s) 2019. CC BY 4.0 License.

Annales Geophysicae Discussions

High-resolution Beijing MST radar detection of tropopause structure and variability over Xianghe (39.75° N, 116.96° E), China

Feilong Chen[1], Gang Chen[1*], Yufang Tian[2], Shaodong Zhang[1], Kaiming Huang[1], Chen Wu[1], Weifan Zhang[1]

[1]School of Electronic Information, Wuhan University, Wuhan 430072, China.

[2]Key Laboratory of Middle Atmosphere and Global Environment Observation, Institute of Atmospheric Physics, Chinese Academy of Sciences, Beijing 100029, China.

*Corresponding author: Gang Chen (g.chen@whu.edu.cn)

Abstract.

As a result of partial specular reflection from the atmospheric stable layer, the radar tropopause (RT) can simply and directly be detected by VHF radars with vertical incidence. Here, the Beijing MST radar measurements are used to investigate the structure and the variabilities of the tropopause in Xianghe, China with a temporal resolution of 0.5 hour from November 2011 to May 2017. High-resolution radar-derived tropopause is compared with the thermal lapse-rate tropopause (LRT) that defined by the World Meteorological Organization (WMO) criterion from twice daily radiosonde soundings and with the dynamical potential vorticity tropopause (PVT) that defined as the height of 2 PVU surface. During all the seasons, the RT and the LRT in altitude agree well with each other with a correlation coefficient of $\geq$0.74. Statistically, weaker (higher) tropopause sharpness seems to contribute to larger (smaller) difference between the RT and the LRT in altitude. The RT agrees well with the PVT in altitude during winter and spring with a correlation coefficient of $\geq$0.72, while the correlation

Ann. Geophys. Discuss., https://doi.org/10.5194/angeo-2018-137
Manuscript under review for journal Ann. Geophys.
Discussion started: 23 January 2019
© Author(s) 2019. CC BY 4.0 License.

Annales Geophysicae Discussions

coefficient in summer is only 0.33. As expected, the monthly mean RT and LRT height both show seasonal variations. Lomb-Scargle periodograms show that the tropopause exhibits obvious diurnal variation throughout the seasons, whereas the semidiurnal oscillations are rare and occasionally observed during summer and later spring. Our study shows the good capability of the Beijing MST radar to determine the tropopause height, as well as present its diurnal oscillations.

Key words: VHF radar; MST radar; tropopause; diurnal oscillation.

1. Introduction

The tropopause marks a transition zone separating the well-mixed convectively active troposphere from the stably stratified and more quiescent stratosphere. Its structure and variability is characterized by large changes in thermal (e.g., lapse rate), dynamical (e.g., potential vorticity), and chemical properties (e.g., ozone and water vapor) and hence acts as a key role for the stratosphere-troposphere exchange (STE) processes (Hoinka, 1998; Seidel et l., 2001). The height of the tropopause depends significantly on the latitude, with about 17 km near the equator and less than 9-10 km at polar latitudes (Ramakrishnan, 1933). Over subtropical latitudes with the presence of subtropical jet, where the tropopause experiences rapid change or breaking, tropopause folding events are commonly observed (Pan et al., 2004). Climatologically, the altitude of the tropopause represents the seasonal variation of the flux of stratospheric air intruding into the troposphere (Appenzeller et al., 1996). Moreover, the tropopause height trends can be a sensitive indicator of anthropogenic climate

Ann. Geophys. Discuss., https://doi.org/10.5194/angeo-2018-137
Manuscript under review for journal Ann. Geophys.
Discussion started: 23 January 2019
© Author(s) 2019. CC BY 4.0 License.

change (Sausen and Santer, 2003; Santer et al., 2003a; Añel et al., 2006).

A variety of ways are available to determine the extratropical tropopause. Radiosonde sounding is the most commonly used to define the thermal tropopause (hereafter referred to as LRT) based on temperature lapse-rate (WMO, 1957). The thermal definition of tropopause can be applied globally and the tropopause height easily be determined from one individual profile (Santer et al., 2003). Radiosonde sounding, however, is impracticable in severe weather conditions such as intense rainfall and cold air outbreak. Another feasible definition is to use a specific potential vorticity (PV) surface to represent the dynamical tropopause (hereafter referred to as PVT) (Reed, 1955; Hoskins et al., 1985). Dynamical definition has the advantage that the PV is a conserved property (under adiabatic and friction-less conditions) of an air mass (Hoskins et al., 1985; Bethan et al., 1996). Values in the range 1-4 PVU (1 PVU= $10^6\ m^2\ s^{-1}\ K\ kg^{-1}$) are used in previous researches in the Northern Hemisphere (e.g. Baray et al., 2000; Sprenger et al., 2003; Hoerling et al., 1991). The threshold of 2 PVU surface is the most commonly used (Gettelman et al., 2011). Dynamical definition, however, is not applicable near the equator, where the PV tends to be 0 (e.g., Hoerling et al., 1991; Nielsen-Gammon et al., 2001).

As a result of partial specular reflection from stable atmospheric layer, the radar tropopause (RT) can be well represented and identified by atmospheric radars operating at meter wavelength (VHF band) and directing at vertical incidence (Gage and Green, 1979). Research activity increased remarkably following the first report on VHF radar detection of tropopause by Gage and Green (1979), for instance, the researches in

Ann. Geophys. Discuss., https://doi.org/10.5194/angeo-2018-137
Manuscript under review for journal Ann. Geophys.
Discussion started: 23 January 2019
© Author(s) 2019. CC BY 4.0 License.

middle latitudes (e.g. Hermawan et al., 1998), polar regions (e.g. Hall, 2013a), and tropical regions (e.g. Das et al., 2008; Ravindrababu et al., 2014). Several methods have been proposed to determine the tropopause height via radar echo power, including the largest gradient in echo power (Vaughan et al., 1995; Alexander et al., 2012), the maximum echo power (Vaughan et al., 1995; Hall et al., 2009), and the specific value of echo power (Gage and Green, 1982; Yamamoto et al., 2003). The method of the RT height determination used in this paper will be described in detail in next section.

The biggest advantage of the VHF radar measurements is the ability of continuous operation unmanned in any weather conditions. Of course, no definition of the tropopause is perfect. VHF radar system can only be limited to a few locations globally. A detailed review of the close relationship between these different tropopause definitions is provided by Alexander et al., (2012).

By means of the radiosonde, reanalysis, and satellite data available globally, long-term (annual or longer) variability in tropopause height has received extensive attention (e.g. Randel et al., 2000; Angell and Korshover, 2009; Son et al., 2011; Liu et al., 2014). However, short period (diurnal or semidiurnal) variability of the tropopause is hard to be examined by these measurements. In contrast, benefiting from the much higher temporal resolution, radar definition of the tropopause provides good capability for studying the diurnal and semidiurnal variation in tropopause height. Earlier, Yamamoto et al., (2003) reported the capability of the Equatorial Atmospheric Radar to examine the diurnal variation of tropopause height. Then, the diurnal variability of the tropical tropopause was investigated in detail by Das et al., (2008) using the Indian Gadanki

Ann. Geophys. Discuss., https://doi.org/10.5194/angeo-2018-137
Manuscript under review for journal Ann. Geophys.
Discussion started: 23 January 2019
© Author(s) 2019. CC BY 4.0 License.

MST radar. Its diurnal variation over a polar latitude station was investigated by Hall (2013b). In the absence of pressure and temperature parameters, the evidence of atmospheric tides can be well represented by winds (e.g. Huang et al., 2015).

The tropopause structure in midlatitudes is different from that in other regions. Double tropopauses structure is a ubiquitous feature over mid-latitude regions near 40°N (Pan et al., 2004; Randel et al., 2007). Strong evidence has revealed that the poleward intrusion of subtropical tropospheric air that occurred above the subtropical jet have resulted in the double structure (Pan et al., 2009). The higher part (second tropopause near ~16 km) is characterized by tropical features of cold and higher level, whereas the lower part (first tropopause near ~12 km) is characterized by polar features of warm and lower level. In the present study, we focus on the first tropopause which will be referred to as 'tropopause' hereafter.

So far, knowledge on the high temporal resolution (within 1 hour) structure and variability of the midlatitude tropopause is still insufficient. In this study, using more than 5 years of Beijing MST radar echo power measurements in vertical beam, we mainly focus on the high-resolution characteristics of the tropopause structure and their comparison with the simultaneous radiosonde and dynamical definitions. Another important objective of this study is to examine the diurnal and semidiurnal variability of the tropopause. The observational characteristics of e.g. winds, echo power, and data acquisition rate near the tropopause layer are also presented in the paper.

2. Data and Methods

Ann. Geophys. Discuss., https://doi.org/10.5194/angeo-2018-137
Manuscript under review for journal Ann. Geophys.
Discussion started: 23 January 2019
© Author(s) 2019. CC BY 4.0 License.

2.1. Radar Dataset

As an important part of the Chinese Meridian Project, two MST radar systems are designed and constructed to improve the understanding of the extratropical troposphere, lower stratosphere, and mesosphere (Wang, 2010), which are Wuhan and Beijing MST radars. The Beijing MST radar located in Xianghe, Hebei Province, China (39.75° N, 116.96° E, 22 m above sea level) was designed and constructed by the Institute of Atmospheric Physics, Chinese Academy of Sciences and started its routine operation since 20 October 2011 (Tian and Lu, 2017). The radar is a high power coherent pulse-Doppler radar operating at 50 MHz with the maximum peak power of 172 kW and the half-power beam width of 3.2°. Five beams are applied: one vertically pointed beam and four 15° off-zenith beams tilted to north, east, south, and west. In order to obtain the high-quality measurements from troposphere, lower stratosphere, and mesosphere simultaneously, the radar is designed to operate routinely in three separate modes: low mode (designed range 2.5-~12 km), middle mode (10-~25 km), and high mode (60-~90 km) with vertical resolutions of 150, 600, and 1200 m, respectively. Under the routine operation, the 15-min break is followed by the 15-min operation cycle (5 min for each mode). As a result, the time resolutions of the low, middle, and high mode measurements are all 30 min. More detailed review of the radar system is given by Chen et al. (2016).

Here only the low mode echo power measurements are used to determine the RT height. Although the designed detectable range of the low mode is from 2.5-~12 km, the vertically pointed beam can receive stronger echoes from a higher level (~14-15 km)

Ann. Geophys. Discuss., https://doi.org/10.5194/angeo-2018-137
Manuscript under review for journal Ann. Geophys.
Discussion started: 23 January 2019
© Author(s) 2019. CC BY 4.0 License.

as compared with those from off-vertical beams due to the partial specular reflection mechanism. The measurements in middle mode are also applied to calculate the winds or echo power within ~5-6 km of the tropopause. The parameters for the two routine operation modes are listed in Table 1. The monthly total number of the echo power profiles available in vertical beam (low mode) is shown in Fig. 1. The outliers or severely contaminated data that mainly induced by system problems are eliminated. The large data gap in September is due to the annual preventive maintenance.

2.2. Tropopause Definitions

Due to the large gradient in potential temperature, radar return power received at vertical incidence is significantly enhanced upon the transition zone of the tropopause layer. Using this characteristic, the RT height can be determined effectively by the VHF radar. Here, the RT is defined as the altitude (above 500 hPa) where the maximum vertical gradient of echo power is located (Vaughan et al., 1995; Alexander et al., 2012; Ravindrababu et al., 2014; Chen et al., 2018). Considering the occasional and random noise, to which the derived-RT is sensitive, the echo power profiles are smoothed by a 3-point running mean. In order to further reduce the influence of the noise, the RT definition used here need to satisfy an additional criterion: the determined RT height should be continuous with the adjacent RT heights (one on each side), otherwise to search for the second peak gradient (eliminated if the second peak does not meet the additional criterion). The “continuous” here means that the discrepancy between the two successive heights (in time, 0.5-hour interval) should be <0.6 km. A typical example of the RT and LRT is illustrated in Fig. 2. The LRT is identified based on the

Ann. Geophys. Discuss., https://doi.org/10.5194/angeo-2018-137
Manuscript under review for journal Ann. Geophys.
Discussion started: 23 January 2019
© Author(s) 2019. CC BY 4.0 License.

World Meteorological Organization (WMO) criteria (WMO, 1957). The radar aspect sensitivity is expressed as the ratio between vertical (p_v) and oblique (p_o) beam echo power (here is 15° east beam). The radiosonde soundings are launched twice daily from the Beijing Meteorological Observatory (39.93 ºN, 116.28 ºE, station number 54511), which is less than 45 km to the radar site. In this case, the LRT and RT consistent well and are at 11.65 km and 11.85 km respectively. As expected, the LRT characterized by a rapid increase in potential temperature gradient also corresponds to the large gradient in radar aspect sensitivity. Note that the height with maximum value in echo power lie at a higher altitude (as compared with the RT height) of ~700 m above the LRT. The dynamical tropopauses used in this paper are derived from the European Centre for Medium-Range Weather Forecasts (ECMWF) ERA-Interim Reanalysis (Dee et al., 2011) and defined as the surface of 2 PVU potential vorticity, which is same to that used by Sprenger et al., (2003) and Alexander et al. (2012).

2.3. Tropopause sharpness definition

For the compared data pairs between the RT and LRT, we calculate the corresponding tropopause sharpness that represents the strength of the tropopause inversion layer. As defined by Wirth, (2000), the tropopause sharpness S_{TP} can be calculated as:

$$S_{TP}=\frac{T_{TP+\Delta z}-T_{TP}}{\Delta z}-\frac{T_{TP}-T_{TP-\Delta z}}{\Delta z} \quad (1)$$

where TP denotes the tropopause height, Δz =1 km, and T_{TP} indicates the corresponding temperature. This definition is also used in Alexander et al. 2012 and we're using it for a good comparison with our results.

Ann. Geophys. Discuss., https://doi.org/10.5194/angeo-2018-137
Manuscript under review for journal Ann. Geophys.
Discussion started: 23 January 2019
© Author(s) 2019. CC BY 4.0 License.

178

179 **3. Results**

180 **3.1. High-resolution radar tropopause structure**

181 The fine-scale height-time cross section of radar echo power and aspect sensitivity
182 is shown in Fig. 3 for a typical month (February 2014), along with the RT, PVT and
183 LRT marked in the figure. In general, the RT agreed well with both the LRT and PVT
184 in height, and most of the RT exhibit a slightly higher altitude. However, the differences
185 between the RT and LRT are sometimes large (reach to ~1-2 km) especially when the
186 RT experience rapid change. Regardless of the background synoptic condition, the
187 difference in the definitions themselves is to a large degree the main contributing factor
188 for the large difference between the RT and LRT. For example, a second layer with
189 significant enhanced echo power is observed above the radar-derived RT for the cases
190 on 4 and 5 February 2012 (Fig.3a). According to the definitions, the RT well defined as
191 the first layer with echo enhanced and the LRT matched the second layer, similar to that
192 observed by Yamamoto et al., (2003) and Fukao et al., (2003). It is of note that the RT
193 well separates the troposphere characterized by low aspect sensitivity from the lower-
194 stratosphere characterized by high aspect sensitivity (Fig.3b).

195 **3.2. Comparisons between different definitions**

196 To further quantify the consistency and difference in altitude between different
197 tropopause definitions, a detailed comparison is carried out in this section. The seasonal
198 scatterplots for RT versus LRT and the histogram distribution of altitude differences
199 between the RT and LRT are illustrated in Fig. 4, during the period November 2011-

Ann. Geophys. Discuss., https://doi.org/10.5194/angeo-2018-137
Manuscript under review for journal Ann. Geophys.
Discussion started: 23 January 2019
© Author(s) 2019. CC BY 4.0 License.

May 2017. A total of 2411 data pairs are obtained for comparison. Among them, the number of data pairs is 845 for DJF (winter), 721 for MAM (spring), 321 for JJA (summer), and 524 for SON (autumn). Comparisons have shown a good consistency throughout the seasons and most of the RTs exhibit a slightly higher than the LRTs. The correlation coefficient is 0.74, 0.80, 0.82, and 0.78 for DJF, MAM, JJA, and SON, respectively. The mean and standard deviation difference (RT minus LRT) calculated in DJF, MAM, JJA, and SON is (0.14 ± 0.75), (0.26 ± 0.78), (0.33 ± 0.56), and (0.12 ± 0.69) km, respectively. The proportion of the data pairs with differences <500 m is reasonably good during four seasons and is 63%, 61%, 64%, and 67% for DJF, MAM, JJA, and SON, respectively. Fig. 4 explicitly indicates the good capability of the Beijing MST radar to determine the tropopause structure well throughout the seasons.

To examine the potential role of the sharpness, Fig. 5a and Fig. 5b show the histogram distribution of the tropopause sharpness along with the probability density curve for data pairs with difference (absolute values of RT minus LRT) <0.5 km and >1 km respectively. What is apparent is that most data pairs of Fig. 5a are located to the right (higher sharpness values, with the peak of ~7.06 K/km) and of Fig. 5b are to the left (lower sharpness values, with the peak of ~6.35 K/km). No matter whether this distribution feature is associated with the cyclonic-anticyclonic systems (e.g. Randel et al., 2007; Randel and Wu, 2010), the results more or less demonstrate that the larger (weaker) tropopause sharpness contribute to lower (higher) difference between the RT and LRT. From the perspective of seasonal statistics, the tropopause sharpness over Beijing station shows similar distribution characteristics throughout the seasons (not

Ann. Geophys. Discuss., https://doi.org/10.5194/angeo-2018-137
Manuscript under review for journal Ann. Geophys.
Discussion started: 23 January 2019
© Author(s) 2019. CC BY 4.0 License.

shown), which is different from that in polar regions where the sharpness is significantly higher during summer than during winter (Zängl and Hoinka, 2001).

The seasonal scatterplots and height difference distribution between the RT and PVT are illustrated and quantified in Fig. 6. The total number of comparing data pairs for winter, spring, summer, and autumn is 1422, 1260, 791, and 1145, respectively. During winter and spring (Fig. 6a and 6b), the RTs agree reasonably well with the PVTs with the correlation coefficient of 0.72 and 0.76 and the mean difference (RT minus PVT) of (0.55±0.84 km) and (1±0.89 km), respectively. In contrast, the consistency for summer and autumn (Fig. 6c and 6d) is relatively bad and with correlation coefficient of 0.33 and 0.47 and mean difference of (0.80±1.39 km) and (0.75±1.23 km), respectively. Especially for summer, the proportion of the comparing data pairs with difference <0.5 km is only 10.6% (84). In autumn, need to note that most data pairs with poor consistency is sampled during early autumn.

3.3. Observational characteristics in the vicinity of the tropopause

Measurements of radar middle mode are used for examining the horizontal wind, return power, and effective data acquisition rate within 5-6 km of the tropopause (upper troposphere and lower stratosphere). Left panels of Fig. 7 show the vertical scatterplots of the static stability (represented by the buoyancy frequency squared) as a function of height relative to the LRT and the right panels show the radar echo power as a function of height relative to the RT, during two specific years 2012-2013 for extended winter NDJFM and summer MJJAS seasons. Results clearly demonstrate the sudden jump in static stability and rapid increase in echo power upon the corresponding tropopause

Ann. Geophys. Discuss., https://doi.org/10.5194/angeo-2018-137
Manuscript under review for journal Ann. Geophys.
Discussion started: 23 January 2019
© Author(s) 2019. CC BY 4.0 License.

244 layer. The variation in echo power is more gradual. The amplitude of both the jump and
245 the increase experienced a slightly larger during NDJFM than that during MJJAS.
246 Fig. 8 shows the profiles of mean radar effective data acquisition rate for low and
247 middle modes during November 2011-May 2017. Here, the "effective data" of one
248 specific range gate requires at least three non-coplanar beams have received
249 backscattered echoes, by which 3-dimensional wind can be derived. The mean data
250 acquisition rate profiles both exhibit an obvious inversion layer (i.e. increase
251 significantly with height) near the tropopause, with the first peak located ~1 km higher
252 above the mean tropopause height. Note that the second inversion in middle mode
253 profile that occurred near 16 km is associated with the second tropopause. As limited
254 by the highest detectable altitude (the data acquisition rate decreased to lower than 20%
255 at ~16 km), the profile in low mode shows little evidence of second inversion.
256 Fig. 9 shows time-height intensity plot of the monthly mean radar-derived
257 horizontal wind (from middle mode) during November 2011-May 2017, together with
258 the monthly mean location of RT and LRT. One pixel grid denotes 1 month×0.6 km.
259 The monthly mean RT and LRT agreed well with each other in height, within 400 m in
260 August and September and even lower in other months of about within 200 m. They
261 both exhibit a clear seasonal variation, with maximum in early autumn of ~11.6 km and
262 minimum in early spring of ~10.3 km. The monthly mean wind jet varies with season,
263 with the thinnest thickness and lowest strength in summer. The mean tropopause height
264 appears to correspond to the lower boundary location of peak wind layer. The error bars
265 of both the RT and LRT help to illustrate that the tropopauses changes by larger

Ann. Geophys. Discuss., https://doi.org/10.5194/angeo-2018-137
Manuscript under review for journal Ann. Geophys.
Discussion started: 23 January 2019
© Author(s) 2019. CC BY 4.0 License.

amplitude in winter and June than that in other months.

3.4. Periodogram analysis of the radar tropopause

High temporal resolution detection of tropopause by VHF radar have allowed us to investigate the diurnal or semidiurnal variability of the tropopause. Atmospheric tides are well known global oscillations contributing to the diurnal variation in temperature and background winds, which in turn modulate the tropopause height. With the absence of high resolution temperature measurements, radar-derived winds are combined used to represent the evidence of diurnal or semidiurnal variation in tropopause height that modulated by tidal. The frequency power spectrum of the RT height, zonal and meridional wind, calculated by means of Lomb-Scargle method (Press and Rybicki, 1989), is illustrated in Fig. 10 for two typical months: May 2015 and December 2016. The choice of Lomb-Scargle algorithm is due to the presence of data gaps (~2 days per week, especially during 2012-2013). The dominant ~24 h periodicity in RT height, zonal and meridional wind is obvious for both months. The evidence of ~12 h period in all three parameters is distinct for May 2015 (Fig. 10a), although the power is relatively weaker. Through the analysis for each individual month, we found that the semidiurnal component in the three parameters is generally and occasionally observed in summer and later spring during our experimental period. The characteristics of the diurnal variation of the RT height can be represented better in Fig. 11, which shows the mean Lomb-Scargle power spectrum of the RT as a function month during November 2011-May 2017. As compared with other months, the dominant diurnal periodicity is less evident in April. We need to clarify that atmospheric tides are of course not the only

Ann. Geophys. Discuss., https://doi.org/10.5194/angeo-2018-137
Manuscript under review for journal Ann. Geophys.
Discussion started: 23 January 2019
© Author(s) 2019. CC BY 4.0 License.

288 source of the diurnal variation in tropopause height, diurnal convective activities
289 (Yamamoto et al., 2003) might also be an important cause. Here will not be detailly
290 discussed.
291
292 **4. Discussion**
293 As for the radar echo power definition, the RT estimation sometimes will fail due
294 to the system problems, even if the thermal tropopause is well defined (Hall et al., 2009).
295 Apart from the system problems, the following two conditions are primarily responsible
296 for the failure (or difficulty) of both the radar and thermal definitions over the radar site
297 latitude (~40° N). Firstly, the temperature sometimes continue to decrease upon into the
298 lower stratosphere (below 16 km) in summer and early autumn, leading to the
299 failure/difficulty of both the radar and thermal definitions (a typical case as shown in
300 Fig. 12a). Need to note that the temperature inversion layer occurred at ~16 km in
301 summer or early autumn is the second tropopause with characteristics of Tropics (Pan
302 et al., 2004; Randel et al., 2007). Secondly, some specific meteorological processes can
303 lead to the ambiguities and indefiniteness in thermal and radar definitions, such as
304 fronts, cyclones or typhoons, and folding (e.g. Nastrom et al., 1989; May et al., 1991;
305 Roettger, 2001; Alexander et al., 2013). Such ambiguities often result in large difference
306 in altitude between the RT and LRT. Especially when multiple temperature inversion
307 layers occurred (below 16 km), the RT generally matched the lower part and LRT often
308 matched the upper part (e.g. Yamamoto et al., 2003; Fukao et al., 2003), such as the
309 double layers of enhanced echo power shown in Fig. 3 on 4 and 5 February 2012. Apart

Ann. Geophys. Discuss., https://doi.org/10.5194/angeo-2018-137
Manuscript under review for journal Ann. Geophys.
Discussion started: 23 January 2019
© Author(s) 2019. CC BY 4.0 License.

310 from the two situations above, there is another condition that is commonly responsible
311 for the failure of thermal definition in summer and early autumn. As the typical case
312 shown in Fig. 12b, a significant inversion in temperature (at ~12 km) is recorded from
313 the radiosonde profile, but this inversion layer is too thin and weak to meet the WMO
314 criterion that thermal definition required. Whereas, the apparent enhancement in radar
315 echo power corresponding to such inversion layer is strong enough to well define the
316 RT. Need to highlight again that the temperature inversion layer that occurred near ~16
317 km is the second tropopause (not considered here). The conditions mentioned above are
318 the main reasons for fewer comparison data pairs in summer than that in other seasons
319 (Fig. 4c and Fig. 6c).

320 Pan et al., (2004) have reported that the difference between the LRT and PVT are
321 more distinct in the vicinity of subtropical jet. In the northern hemisphere, the axis of
322 the subtropical jet is situated near ~30°N in spring and winter, whereas in summer and
323 early autumn the subtropical jet shifts northward to ~40°N (see Fig. 4 in Ding and Wang,
324 2006). We preliminary considered that the bad consistency between the RT and PVT in
325 summer and early autumn (Fig. 6c and 6d) is most likely associated with the subtropical
326 jet shifting poleward to ~40°N. The existing cyclones or anticyclones in the upper-
327 troposphere (Wirth, 2000), of course, may also be an important cause of the significant
328 asymmetric differences (scattered points deviate significantly from the 1:1 line and
329 PVT located below the RT in most cases, as shown in Fig. 6c). More detailed discussion
330 about the striking asymmetric differences in height between LRT and PVT can be seen
331 in Wirth (2001). Anyway, we need to be careful when using the dynamical definition to

Ann. Geophys. Discuss., https://doi.org/10.5194/angeo-2018-137
Manuscript under review for journal Ann. Geophys.
Discussion started: 23 January 2019
© Author(s) 2019. CC BY 4.0 License.

define the tropopause over radar site latitude ~40° N, especially in summer.

About the characteristics of tropopause and the comparison between different definitions, there are many differences between mid-latitude and polar regions. In mid-latitude (~40°N), our results show that: (1) the agreement between RT and LRT is similar good throughout the seasons; (2) RTs are generally located higher than the LRT; (3) the thermal definition sometimes fail in summer and early autumn; (4) the agreement between the RT/LRT and PVT in summer is poor. Whereas, in contrast, previous researches about the tropopause over polar regions showed that (Wirth, 2000；Alexander et al., 2012): (1) the difference between the RT and LRT is larger during winter than that during summer; (2) RTs are generally located lower than the LRT; (3) the thermal definition sometimes fail in winter and spring; (4) comparison between the RT and PVT showed the similar good agreement during both summer and winter.

Over a polar latitude station, the seasonal characteristics of the diurnal oscillation in tropopause height were investigated using 5 years of SOUSY VHF radar measurements (Hall, 2013b). The sunlight variability in polar regions is different from that in other latitudes of the world. Different sunlight variation actually will lead to difference in atmospheric tides, and then would result in different diurnal variation in tropopause height. Here we found that the diurnal oscillation of RT height at Xianghe is ubiquitous and obvious throughout the seasons except for April (Fig. 11). Whereas at polar latitude and in months of November to February when there is no sunlight, Hall (2013b) observed little evidence of 24 h diurnal variability in RT height.

Ann. Geophys. Discuss., https://doi.org/10.5194/angeo-2018-137
Manuscript under review for journal Ann. Geophys.
Discussion started: 23 January 2019
© Author(s) 2019. CC BY 4.0 License.

5. Conclusions

In this paper, we present the high resolution structure and variability of the tropopause in Xianghe, China (39.75° N, 116.96° E), based on the Beijing MST radar vertical beam echo power data collected during the period November 2011-May 2017. Fine-scale structure of the RT is well determined with a high temporal resolution of 0.5 h. Comparison results have shown good agreement in altitude between the RT and LRT, with a correlation coefficient of ≥ 0.74 for the four seasons. Higher tropopause sharpness seems to contribute lower difference between the RT and LRT in altitude and weaker sharpness appears responsible for higher difference. The agreement between the RT and PVT is relatively well in winter and spring with correlation coefficient of 0.72 and 0.76 respectively, but poor during summer with a correlation coefficient of only 0.33. We initially suggested that the poor consistency between RT and PVT is associated with the subtropical jet shifting poleward to ~40°N.

As expected, the sudden jump in static stability (represented by the buoyancy frequency squared) and the rapid increase in radar echo power upon the tropopause layer are clearly observed. A significant inversion (increasing with height) in effective radar data acquisition rate is also observed upon the tropopause layer. Both the monthly mean RT and LRT height have shown a clear annual cycle. The variability and oscillation of RT height with diurnal or lower timescales is presented. Obvious diurnal variation in tropopause height, zonal wind, and meridional wind is generally observed throughout the seasons, indicating the modulation most likely from the atmospheric tides. The semidiurnal variation in RT height is not so obvious and commonly observed

© Author(s) 2019. CC BY 4.0 License.

376 occasionally in summer and late spring.

377

378 **Acknowledgment**

379 This work is funded by National Natural Science Foundation of China (NSFC grants
380 No. 41474132 and 41722404). We acknowledge the Chinese Meridian Project for
381 providing the MST radar data. The authors sincerely acknowledge the ECMWF for
382 providing global reanalysis data. The MST radar data for this paper are available at
383 Data Centre for Meridian Space Weather Monitoring Project (http://159.226.22.74/).
384 The radiosonde data are publicly available from the NOAA/ESRL Database at
385 https://ruc.noaa.gov/raobs/.

386

387 **References**

388 Alexander, S. P., Murphy, D. J., and Klekociuk, A. R.: High resolution VHF radar
389 measurements of tropopause structure and variability at Davis, Antarctica (69° S,
390 78° E). Atmospheric Chemistry and Physics, 12(10), 26173-26205, 2012.
391 Angell, J. K., and Korshover, J.: Quasi-biennial and long-term fluctuations in
392 tropopause pressure and temperature, and the relation to stratospheric water vapor
393 content. Monthly Weather Review, 102(1), 29-34, 2009.
394 Appenzeller, C., Holton, J. R., and Rosenlof, K. H.: Seasonal Variation of Mass
395 Transport Across the Tropopause. Journal of Geophysical Research, 101(D10),
396 15071-15078, 1996.
397 Añel, J. A., J. C. Antuña, L. de la Torre, R. Nieto, and Gimeno L.: Changes in

© Author(s) 2019. CC BY 4.0 License.

tropopause height for the Eurasian region determined from CARDS radiosonde data. Naturwissenschafte, 93, 603–609, doi:10.1007/s00114-006-0147-5, 2006.

Bethan, S., Vaughan, G., and Reid, S. J.: A comparison of ozone and thermal tropopause heights and the impact of tropopause definition on quantifying the ozone content of the troposphere. Quarterly Journal of the Royal Meteorological Society, 122(532), 929-944, 1996.

Baray, J., Daniel, V., Ancellet, G., and Legras, B.: Planetary-scale tropopause folds in the southern subtropics. Geophysical Research Letters, 27(3), 353-356, 2000.

Chen, F. L., Chen, G., Shi, C. H., Tian, Y. F., Zhang, S. D., and Huang, K. M.: Strong downdrafts preceding rapid tropopause ascent and their potential to identify cross-tropopause stratospheric intrusions, Annales Geophysicae, 36(5), 1403-1417, 2018.

Chen, G., Cui, X., Chen, F., Zhao, Z., Wang, Y., Yao, Q., and Gong, W.: MST Radars of Chinese Meridian Project: System Description and Atmospheric Wind Measurement. IEEE Transactions on Geoscience and Remote Sensing, 54(8), 4513-4523, 2016.

Das, S. S., Jain, A. R., Kumar, K. K., and Rao, D. N.: Diurnal variability of the tropical tropopause: Significance of VHF radar measurements. Radio Science, 43(6), 1-14, doi:10.1029/2008RS003824, 2008.

Dee, D. P., Uppala, S. M., Simmons, A. J., Berrisford, P., Poli, P., Kobayashi, S. et al.: The ERA-Interim reanalysis: configuration and performance of the data assimilation system. Quarterly Journal of the Royal Meteorological Society,

© Author(s) 2019. CC BY 4.0 License.

137(656), 553-597, 2011.

Ding, A., and Wang, T.: Influence of stratosphere-to-troposphere exchange on the seasonal cycle of surface ozone at Mount Waliguan in western China. Geophysical Research Letters, 33(3), 233-252, doi:10.1029/ 2005GL024760, 2006.

Fukao, S., H. Hashiguchi, M. Yamamoto, T. Tsuda, T. Nakamura, M. K. Yamamoto, T. Sato, M. Hagio, and Y. Yabugaki:. Equatorial Atmosphere Radar (EAR): System description and first results. Radio Science, 38(3), 1053, 2003.

Gage, K. S., and Green, J. L.: An objective method for the determination of tropopause height from VHF radar observations. Journal of Applied Meteorology, 21(21), 1150-1154, 1982.

Gage, K. S., and Green, J. L.: Tropopause Detection by Partial Specular Reflection with Very-High-Frequency Radar. Science, 203(4386), 1238-1240, 1979.

Gettelman, A., P. Hoor, L. L. Pan, W. J. Randel, M. I. Hegglin, and T. Birner: The extratropical upper troposphere and lower stratosphere, Reviews of Geophysics, 49(3), RG3003, doi: 10.1029/2011RG000355, 2011.

Hermawan, E., Tsuda, T., and Adachi, T.: MU radar observations of tropopause variations by using clear air echo characteristics. Earth, Planets and Space, 50(4), 361-370, 1998.

Hall, C.: The radar tropopause above Svalbard 2008–2012: Characteristics at various timescales. Journal of Geophysical Research, 118(6), 2600-2608, 2013a.

Hall, C.: The radar tropopause at 78°N, 16°E: Characteristics of diurnal variation. Journal of Geophysical Research, 118(12), 6354-6359, doi:10.1002/jgrd.50560,

© Author(s) 2019. CC BY 4.0 License.

2013b.

Hall, C. M., Röttger, J., Kuyeng, K., Sigernes, F., Claes, S., and Chau, J. L.: Tropopause altitude detection at 78°N, 16°E, 2008: First results of the refurbished SOUSY radar. Radio Science, 44(5), 1-12, doi:10.1029/ 2009RS004144, 2009.

Hoinka, K. P.: Statistics of the Global Tropopause Pressure. Monthly Weather Review, 126(12), 3303-3325, 1998.

Hoskins, B. J., Mcintyre, M. E., and Robertson, A. W.: On the use and significance of isentropic potential vorticity maps. Quarterly Journal of the Royal Meteorological Society, 111(470), 877-946, 2007.

Huang, C., Zhang, S. D., Zhou, Q. H., Yi, F., Huang, K., Gong, Y., Zhang, Y., and Gan, Q.: WHU VHF radar observations of the diurnal tide and its variability in the lower atmosphere over Chongyang (114.14° E, 29.53° N), China. Annales Geophysicae, 33(7), 865-874, 2015.

Hoerling, M. P., Schaack, T. K., and Lenzen, A. J.: Global Objective Tropopause Analysis. Monthly Weather Review, 119(8), 1816-1831, 1991.

Liu, Y., Xu, T., and Liu, J.: Characteristics of the seasonal variation of the global tropopause revealed by cosmic/GPS data. Advances in Space Research, 54(11), 2274-2285, 2014.

May, P. T., Yamamoto, M., Fukao, S., Sato, T., Kato, S., and Tsuda, T.: Wind and reflectivity fields around fronts observed with a VHF radar. Radio Science, 26(5), 1245-1249, 1991.

© Author(s) 2019. CC BY 4.0 License.

463 Nastrom, G. D., Green, J. L., Gage, K. S., and Peterson, M. R.: Tropopause Folding
464 and the Variability of the Tropopause Height as Seen by the Flatland VHF Radar.
465 Journal of Applied Meteorology, 28(12), 1271-1281, 1989.
466 Nielsen-Gammon, J. W.: A visualization of the global dynamic tropopause. Bulletin of
467 the American Meteorological Society, 82(6), 1151-1168, 2001.
468 Pan, L. L., Randel, W. J., Gary, B. L., Mahoney, M. J., and Hintsa, E. J.: Definitions
469 and sharpness of the extratropical tropopause: A trace gas perspective. Journal of
470 Geophysical Research, 109, D23103, doi:10.1029/2004JD004982, 2004.
471 Pan, L. L., W. J. Randel, J. C. Gille, W. D. Hall, B. Nardi, S. Massie, V. Yudin, R.
472 Khosravi, P. Konopka, and D. Tarasick: Tropospheric intrusions associated with
473 the secondary tropopause, Journal of Geophysical Research, 114, D10302, 2009.
474 Press, W. H., and Rybicki, G. B.: Fast algorithm for spectral analysis of unevenly
475 sampled data. The Astrophysical Journal, 338(1), 277-280, 1989.
476 Ravindrababu, S., Venkat Ratnam, M., Sunilkumar, S. V., Parameswaran, K., and
477 Krishna Murthy, B. V.: Detection of tropopause altitude using Indian MST radar
478 data and comparison with simultaneous radiosonde observations. Journal of
479 Atmospheric and Solar-Terrestrial Physics, 121(6), 679-687, 2014.
480 Randel, W. J., Wu, F., and Gaffen, D. J.: Interannual variability of the tropical
481 tropopause derived from radiosonde data and NCEP reanalyses. Journal of
482 Geophysical Research Atmospheres, 105(D12), 15509-15523, 2000.
483 Randel, W. J., Seidel, D. J., and Pan, L. L.: Observational characteristics of double
484 tropopauses. Journal of Geophysical Research, 112, D07309, 2007.

© Author(s) 2019. CC BY 4.0 License.

485 Randel, W. J., and Wu, F.: The Polar Summer Tropopause Inversion Layer. Journal of
486 the Atmospheric Sciences, 67(8), 2572-2581, 2010.
487 Randel, W. J., Wu, F., and Forster, P. M.: The extratropical tropopause inversion layer:
488 Global observations with GPS data, and a radiative forcing mechanism. Journal of
489 the Atmospheric Sciences, 64(12), 4489-4496, 2007.
490 Ramakrishnan, K. P.: Distortion of the tropopause due to meridional movements in the
491 sub-stratosphere. Nature, 132(3346), 932-932, 1933.
492 Roettger, J.: Observations of the polar d-region and the mesosphere with the Eiscat
493 Svalbard radar and the SOUSY Svalbard Radar (scientific paper). Memoirs of
494 National Institute of Polar Research. Special Issue, 54(94), 9-20, 2001.
495 Reed, R. J.: A study of a characteristic tpye of upper-level frontogenesis. Journal of the
496 Atmospheric Sciences, 12(3), 226-237, 1955.
497 Santer, B. D., Wehner, M. F., Wigley, T. M., Sausen, R., Meehl, G. A., Taylor, K. E.,
498 Ammann, C., Arblaster, J., Washington, W. M., Boyle, J. S., and Brüggemann, W.:
499 Contributions of anthropogenic and natural forcing to recent tropopause height
500 changes. Science, 301(5632), 479-483, 2003.
501 Santer, B. D., Sausen, R., Wigley, T. M., Boyle, J. S., Achutarao, K., Doutriaux, C.,
502 Hansen, J. E., Meehl, G. A., Roeckner, E., Ruedy, R., Schmidt, G., and Taylor, K.
503 E.: Behavior of tropopause height and atmospheric temperature in models,
504 reanalyses, and observations: Decadal changes. Journal of Geophysical Research,
505 108(D1), 4002, doi:10.1029/2002JD002258, 2003a.
506 Sausen, R., and Santer, B. D.: Use of Changes in Tropopause Height to Detect Human

© Author(s) 2019. CC BY 4.0 License.

Influences on Climate. Meteorologische Zeitschrift, 12(3), 131-136, 2003.

Seidel, D. J., Ross, R. J., Angell, J. K., and Reid, G. C.: Climatological characteristics of the tropical tropopause as revealed by radiosondes. Journal of Geophysical Research, 106(D8), 7857-7878, 2001.

Son, S., Tandon, N. F., and Polvani, L. M.: The fine-scale structure of the global tropopause derived from cosmic gps radio occultation measurements. Journal of Geophysical Research Atmospheres, 116, D20113, 2011.

Sprenger, M., Croci Maspoli, M., and Wernli, H.: Tropopause folds and cross-tropopause exchange: a global investigation based upon ECMWF analyses for the time period March 2000 to February 2001. Journal of Geophysical Research Atmospheres, 108(12), 291-302, 2003.

Tian, Y., and Lu, D.: Comparison of Beijing MST Radar and Radiosonde Horizontal Wind Measurements. Advances in Atmospheric Sciences, 34(1), 39-53. doi: 10.1007 / s00376-016-6129-4, 2017.

Vaughan, G., Howells, A., and Price, J. D.: Use of MST radars to probe the mesoscale structure of the tropopause. Tellus A, 47(5), 759-765, 1995.

Wang, C.: Development of the Chinese meridian project. Chinese Journal of Space Science, 30(4), 382–384, 2010.

Wirth, V.: Thermal versus dynamical tropopause in upper-tropospheric balanced flow anomalies. Quarterly Journal of the Royal Meteorological Society, 126(562), 299-317, 2000.

Ann. Geophys. Discuss., https://doi.org/10.5194/angeo-2018-137
Manuscript under review for journal Ann. Geophys.
Discussion started: 23 January 2019
© Author(s) 2019. CC BY 4.0 License.

528 Wirth, V.: Cyclone-anticyclone asymmetry concerning the height of the thermal and the
529 dynamical tropopause. Journal of the Atmospheric Sciences, 58(1), 26-37, 2001.
530 WMO: Definition of the tropopause. WMO Bull., 6, 136, 1957.
531 Yamamoto, M., Oyamatsu, M., Horinouchi, T., Hashiguchi, H., and Fukao, S.: High
532 time resolution determination of the tropical tropopause by the Equatorial
533 Atmosphere Radar. Geophysical Research Letters, 30(21), 2094, 2003.
534 Zängl, G., and Hoinka, K. P.: The tropopause in the polar regions. Journal of Climate,
535 14(2001), 3117-3139, 2001.
536

Ann. Geophys. Discuss., https://doi.org/10.5194/angeo-2018-137
Manuscript under review for journal Ann. Geophys.
Discussion started: 23 January 2019
© Author(s) 2019. CC BY 4.0 License.

Annales Geophysicae Discussions
Open Access
EGU

537 **Table**

Radar parameter	Value
Transmitted frequency	50 MHz
Antenna array	24×24 3-element Yagi
Antenna gain	33 dB
Transmitter peak power	172 kW
Code	16-bit complementary
No. coherent integrations	128 (low mode)/64 (mid mode)
No. FFT points	256
No. spectral average	10
Pulse repetition period	160 (low mode)/320 (mid mode) μs
Half power beam width	3.2^o
Pulse length	1 (low mode)/4 (mid mode) μs
Range resolution	150 (low mode)/600 (mid mode) m
Temporal resolution	30 min
Off-zenith angle	15^o

538 **Table 1.** Routine operational parameters in low and middle mode for the Beijing MST
539 radar used in this study.

540

Ann. Geophys. Discuss., https://doi.org/10.5194/angeo-2018-137
Manuscript under review for journal Ann. Geophys.
Discussion started: 23 January 2019
© Author(s) 2019. CC BY 4.0 License.

Annales Geophysicae Discussions
Open Access
EGU

541 **Figures**

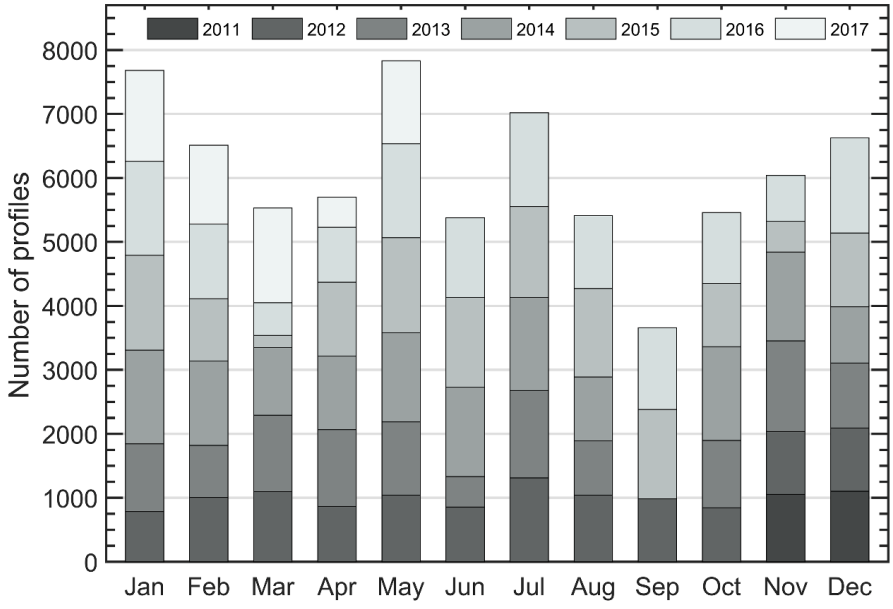

542

543 **Figure 1.** Distribution of the monthly total number of radar return echo power profiles

544 that available from vertical beam in low mode, collected for the period November 2011-

545 May 2017.

Ann. Geophys. Discuss., https://doi.org/10.5194/angeo-2018-137
Manuscript under review for journal Ann. Geophys.
Discussion started: 23 January 2019
© Author(s) 2019. CC BY 4.0 License.

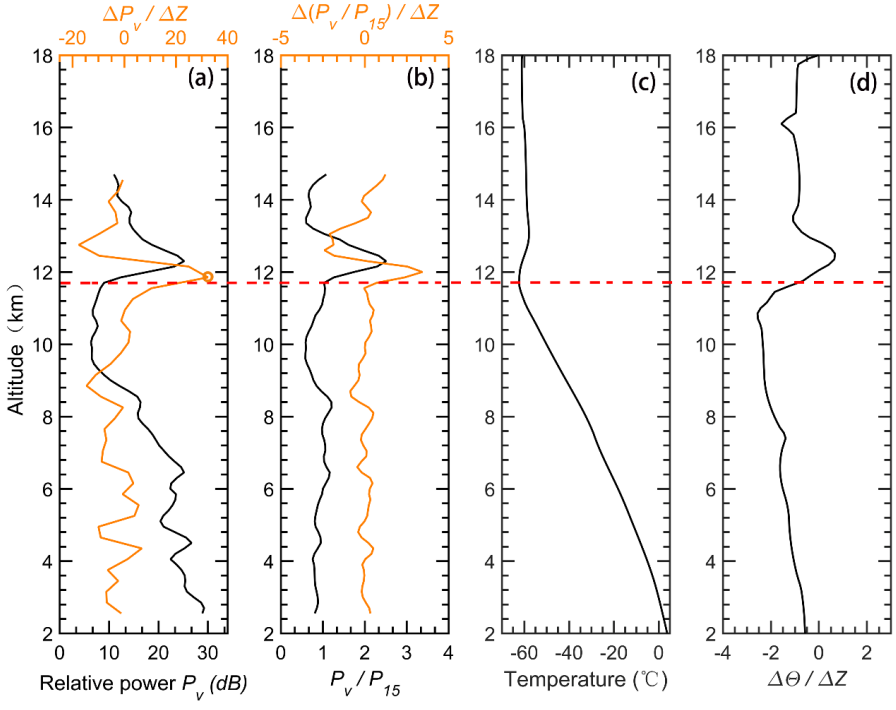

Figure 2. Example vertical profiles of (a) relative radar echo power (black line) along with its gradient variation (orange line), (b) radar aspect sensitivity (black line) along with its gradient variation (orange line), (c) radiosonde temperature and (d) potential temperature gradient on 00 UT 04 November 2011. The horizontal red dashed line marks the LRT height. The orange circle in Fig. 2a denotes the RT height.

Ann. Geophys. Discuss., https://doi.org/10.5194/angeo-2018-137
Manuscript under review for journal Ann. Geophys.
Discussion started: 23 January 2019
© Author(s) 2019. CC BY 4.0 License.

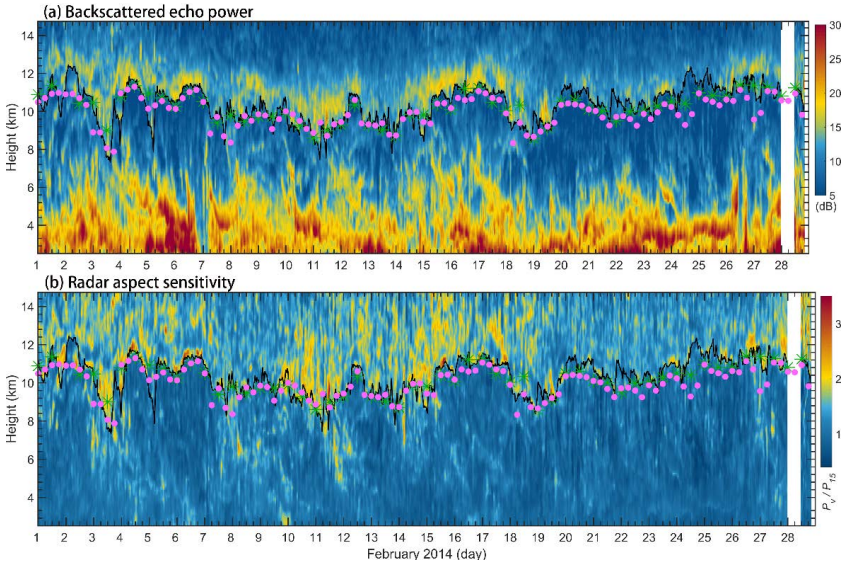

554

555 **Figure 3.** Altitude-time intensity plot of (a) radar backscattered echo power and (b)
556 radar aspect sensitivity for February 2014. The tropopauses determined based on the
557 radar echo definition are shown as a black solid curve. The green asterisks '*' and pink
558 dots indicate the location of the LRT derived from simultaneous twice daily radiosonde
559 data and the PVT from ECMWF ERA-Interim reanalysis, respectively. White stripe
560 indicates the time frame of radar missing data.

561

Ann. Geophys. Discuss., https://doi.org/10.5194/angeo-2018-137
Manuscript under review for journal Ann. Geophys.
Discussion started: 23 January 2019
© Author(s) 2019. CC BY 4.0 License.

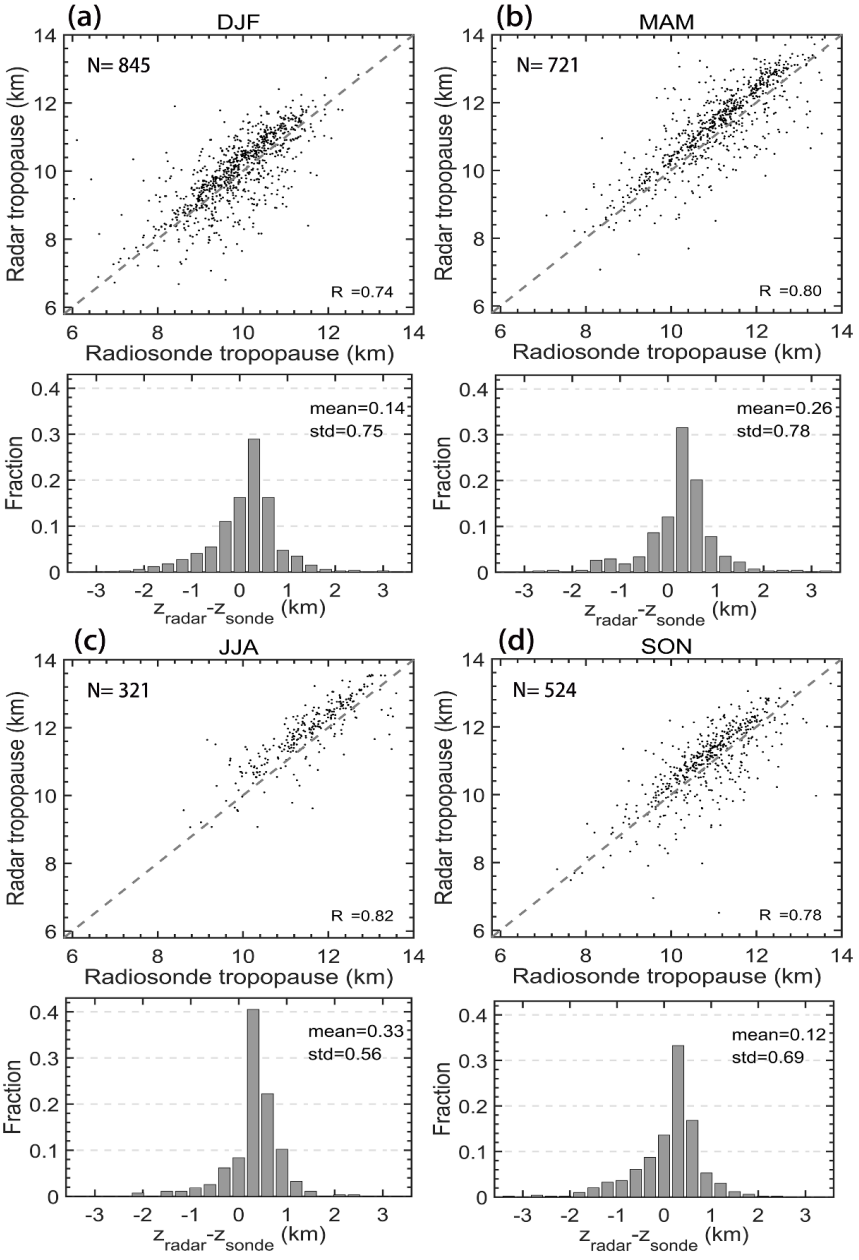

Figure 4. Seasonal scatterplots of the RT versus LRT and histogram distribution of altitude differences between the RT and the LRT, for (a) winter DJF, (b) spring MAM, (c) summer JJA, and (d) autumn SON, during the period November 2011-May 2017.

Ann. Geophys. Discuss., https://doi.org/10.5194/angeo-2018-137
Manuscript under review for journal Ann. Geophys.
Discussion started: 23 January 2019
© Author(s) 2019. CC BY 4.0 License.

566 The positive values in the histogram indicate the RT locating at a higher level than the
567 LRT. The grey dashed line shows the 1:1 line. Here, 'N','R^2', 'mean', and 'std' indicate
568 the sample numbers, correlation coefficient, mean difference, and standard deviation of
569 the difference, respectively.

570

571

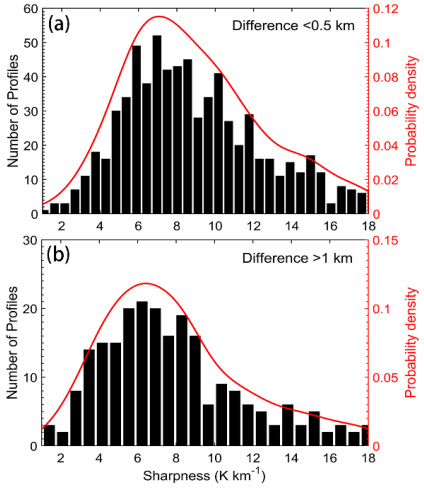

572

573 **Figure 5.** Histogram distribution of the tropopause sharpness for (a) difference <0.5
574 km, and (b) >1 km respectively between the LRT and the RT.

575

Ann. Geophys. Discuss., https://doi.org/10.5194/angeo-2018-137
Manuscript under review for journal Ann. Geophys.
Discussion started: 23 January 2019
© Author(s) 2019. CC BY 4.0 License.

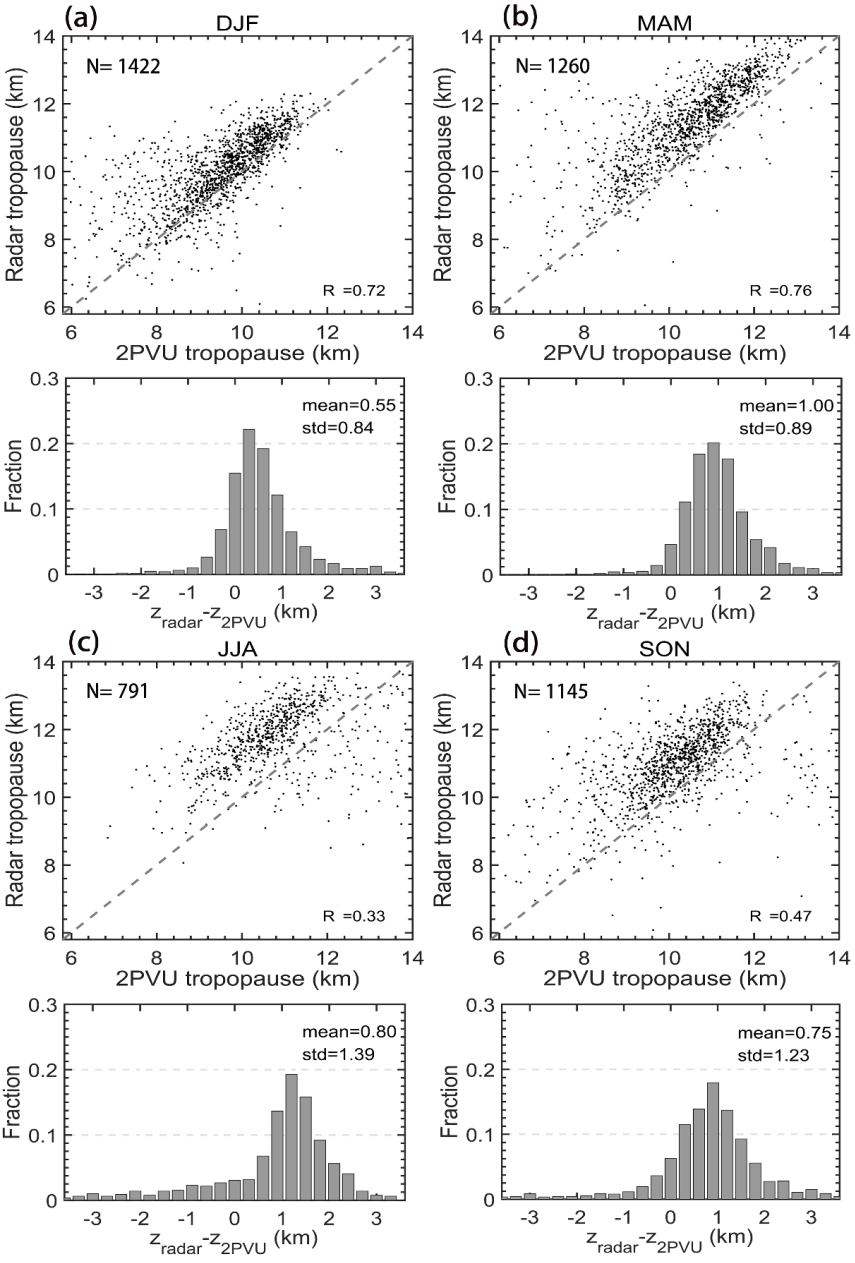

Figure 6. Same as figure 4, but for the comparison between the RT and the PVT.

Ann. Geophys. Discuss., https://doi.org/10.5194/angeo-2018-137
Manuscript under review for journal Ann. Geophys.
Discussion started: 23 January 2019
© Author(s) 2019. CC BY 4.0 License.

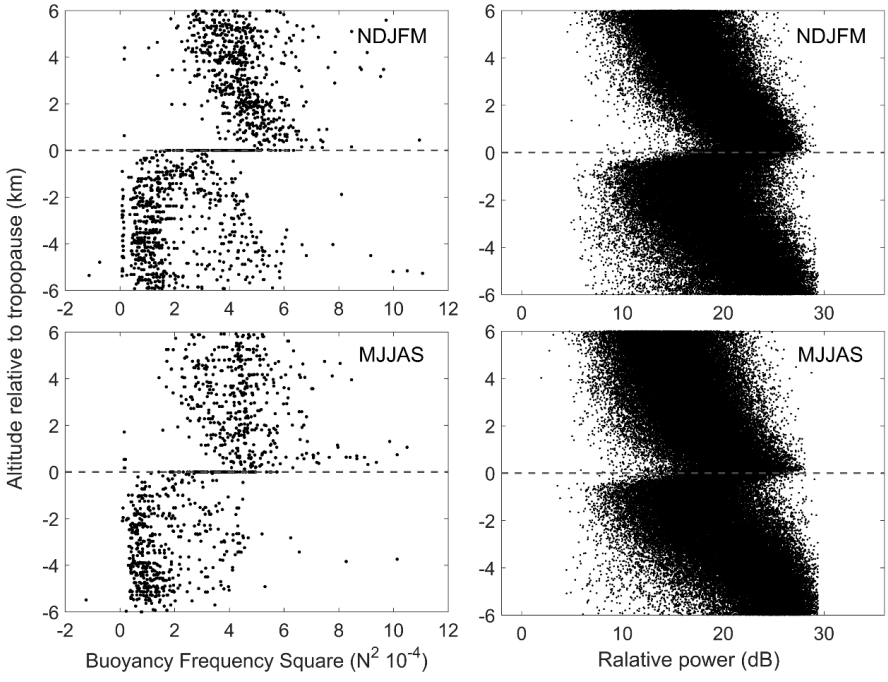

579

580 **Figure 7.** Scatterplots of (left panels) static stability (N^2) and (right panels) radar
581 relative echo power as a function of altitude relative to the LRT (left panels) and RT
582 (right panels) for extended winter (NDJFM) and summer (MJJAS) seasons for two
583 specific years 2012-2013.

584

585

Ann. Geophys. Discuss., https://doi.org/10.5194/angeo-2018-137
Manuscript under review for journal Ann. Geophys.
Discussion started: 23 January 2019
© Author(s) 2019. CC BY 4.0 License.

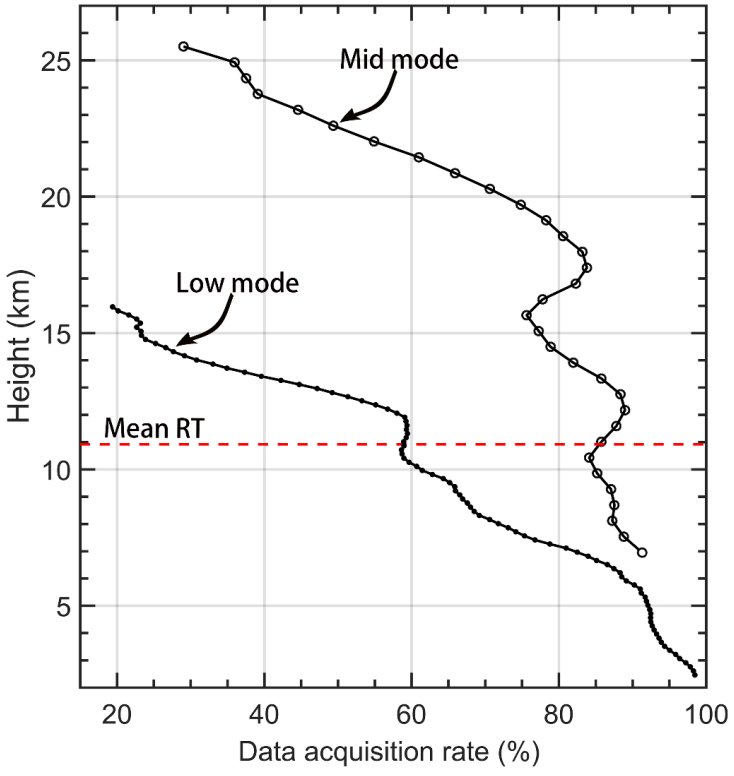

586

587 **Figure 8.** Vertical height profiles of the averaged effective radar data acquisition rate

588 in low mode and middle mode during November 2011-May 2017. The red dashed line

589 indicates the mean RT height.

590

Ann. Geophys. Discuss., https://doi.org/10.5194/angeo-2018-137
Manuscript under review for journal Ann. Geophys.
Discussion started: 23 January 2019
© Author(s) 2019. CC BY 4.0 License.

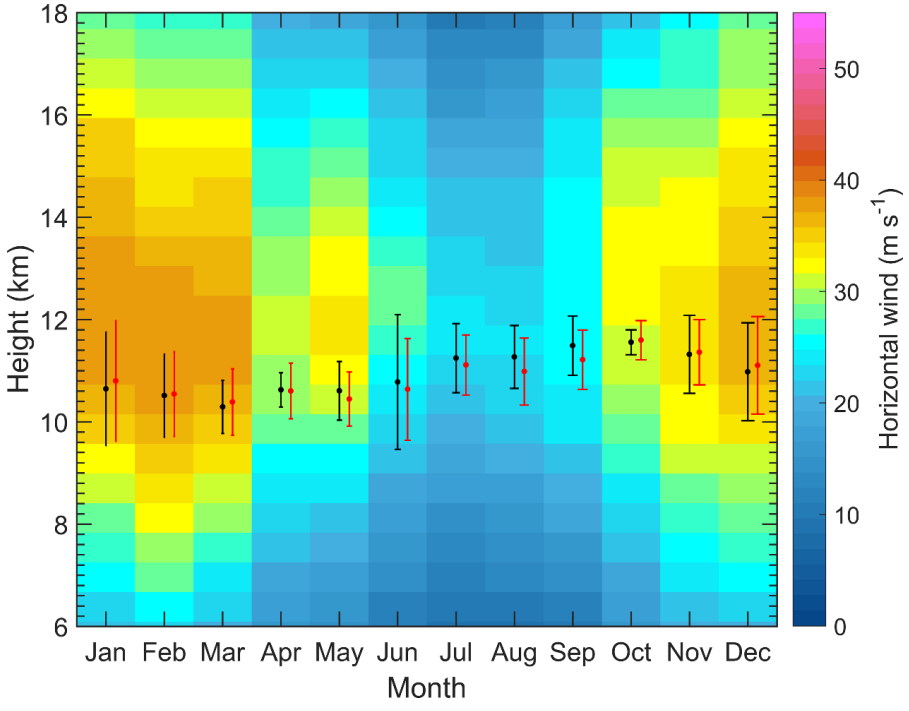

591

592 **Figure 9.** Height-time intensity map of monthly mean horizontal wind speed (shaded,
593 m/s) derived from the middle mode of Beijing MST radar, during November 2011-May
594 2017. Also shown is the monthly mean height of RT (black dots) and LRT (red dots,
595 offset by +6 days) along with the vertical error bars representing the standard deviations.

596

Ann. Geophys. Discuss., https://doi.org/10.5194/angeo-2018-137
Manuscript under review for journal Ann. Geophys.
Discussion started: 23 January 2019
© Author(s) 2019. CC BY 4.0 License.

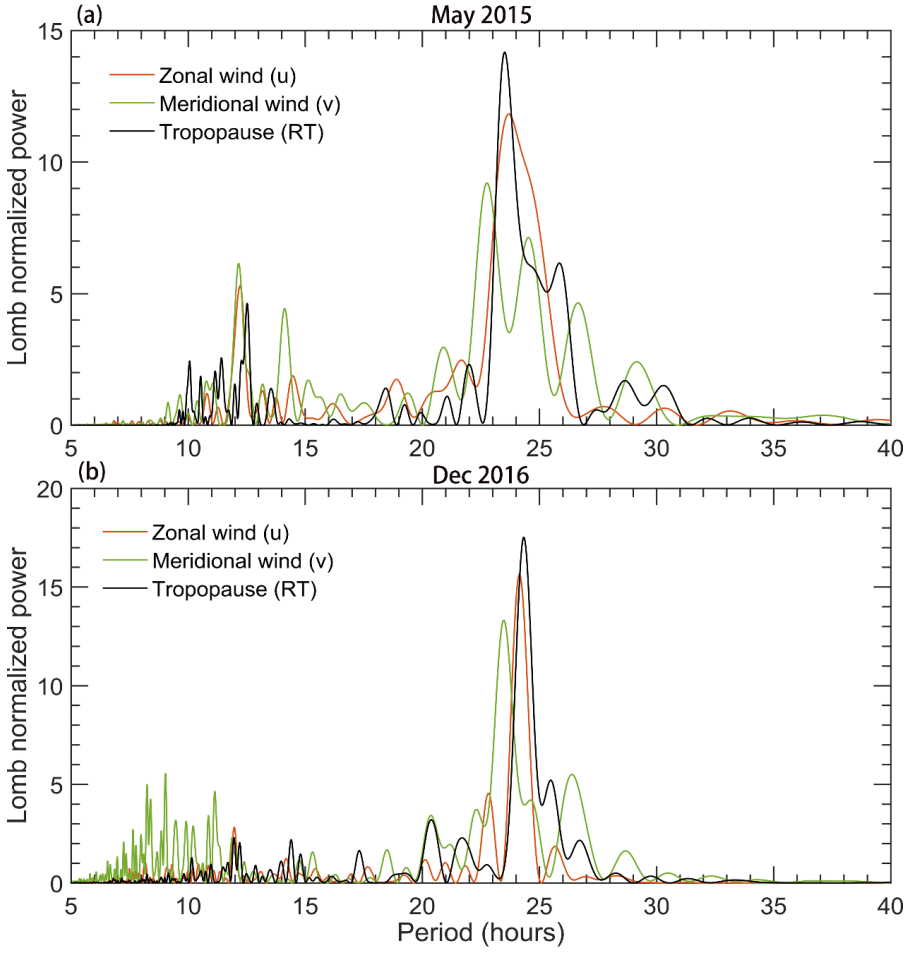

Figure 10. Lomb-Scargle periodograms of the RT height, zonal, and meridional wind oscillations for specific months of (a) May 2015 and (b) December 2016. The zonal and meridional wind for (a) is sampled at 9.85 km and (b) at 11 km.

Ann. Geophys. Discuss., https://doi.org/10.5194/angeo-2018-137
Manuscript under review for journal Ann. Geophys.
Discussion started: 23 January 2019
© Author(s) 2019. CC BY 4.0 License.

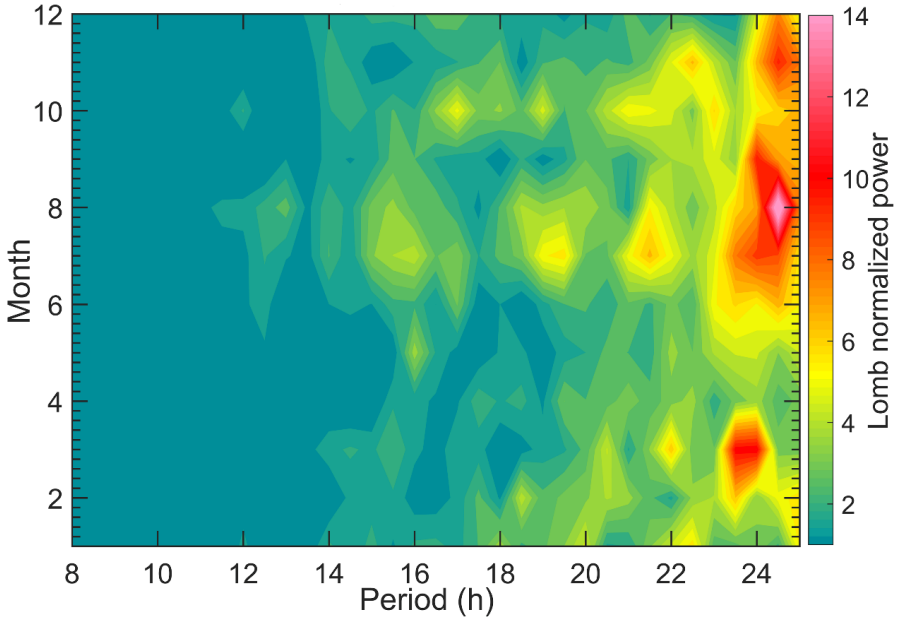

602

603 **Figure 11.** Mean Lomb-Scargle periodograms of RT height as a function of the time of

604 month during November 2011-May 2017.

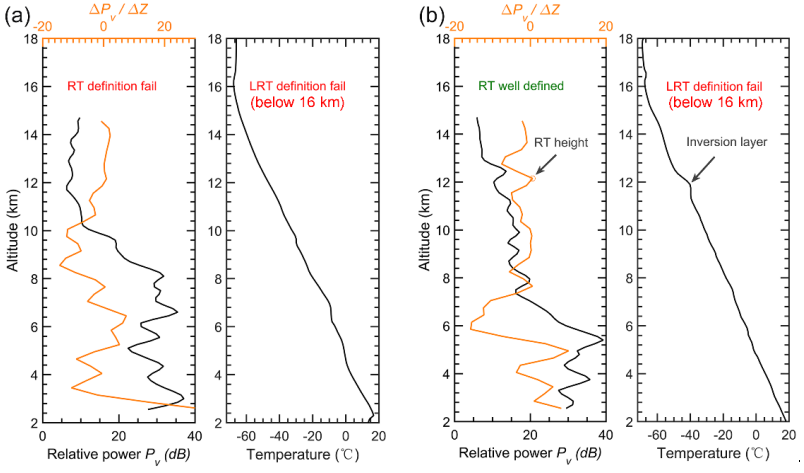

605

606 **Figure 12.** Example profiles of radar echo power and radiosonde temperature that (a)

607 both the RT and LRT definitions fail due to the continuing decrease in temperature on

608 00 UTC 7 July 2012 and (b) the temperature inversion layer failed to meet the LRT

609 definition but well defined in RT definition on 12 UTC 02 August 2012.